ChemBioChem

Review
doi.org/10.1002/cbic.202400754

Chemistry Europe
European Chemical Societies Publishing

www.chembiochem.org

Dynamic Nanostructure-Based DNA Logic Gates for Cancer Diagnosis and Therapy

Shiyi Bi,[a] Ruowen Yang,[a] Huangxian Ju,[a] and Ying Liu*[a, b]

DNA logic gates with dynamic nanostructures have made a profound impact on cancer diagnosis and treatment. Through programming the dynamic structure changes of DNA nanodevices, precise molecular recognition with signal amplification and smart therapeutic strategies have been reported. This enhances the specificity and sensitivity of cancer theranostics, and improves diagnosis precision and treatment outcomes. This review explores the basic components of dynamic DNA nanostructures and corresponding DNA logic gates, as well as their applications for cancer diagnosis and therapies. The dynamic DNA nanostructures would contribute to cancer early detection and personalized treatment.

1. Introduction

Cancer remains one of the leading causes of death worldwide. Traditional diagnostic and therapeutic approaches often suffer from sensitivity and specificity limitations, as well as significant side effects, which impairs treatments efficiency and causes damage to healthy tissues.[1] In recent years, the integration of nanotechnology and molecular biology has opened new opportunities for cancer diagnosis and treatment, where DNA-based nanodevices showing great potential.[2] As a complex and highly heterogeneous disease, cancer development involves multiple intracellular and extracellular processes, which requires precise diagnosis and personalized treatment strategies.[3] Although FDA-approved nanomedicines such as liposomes and polymer nanoparticles are widely used, current nanotechnology still lacks autonomous intelligence.[5] The rapid advancement of nanotechnology, particularly in precision strategies targeting the tumor microenvironment and biomarkers, offers effective solutions.[4]

By leveraging unique base-pairing mechanisms and dynamic assembly capabilities, dynamic DNA nanostructures can respond or adjust according to external stimuli or environmental changes.[6] With dynamic DNA nanostructures as main components, the DNA logic circuit can be conceptualized as a black box, which accepts specific biomarkers as input signals, implements signal conversion by performing logical judgment and signal amplification, and finally releases output signals.[7,8] Dynamic DNA nanostructure-based DNA logic circuits could enhance the intelligence of nanomedicine, thus show broad application prospects in bioimaging, and drug loading/release.[9]

This review introduces the basic components of dynamic DNA nanostructures and the advancements in developing DNA logic gates based on these structures, with a focus on their applications in cancer diagnostics and therapy. We highlight recent innovations in the design and functionality of these systems, discuss the challenges that remain in their clinical translation, and propose potential future directions for research in this rapidly evolving field.

2. Basic Components of Dynamic DNA Nanostructures

We briefly reviewed dynamic DNA nanostructures that have been utilized in DNA logic circuits.

2.1. DNA Strand Displacement Reactions

DNA strand displacement reactions are the major component for dynamic DNA nanostructure-based DNA logic gates.[10] In these reactions, an "input" DNA strand interacts with a pre-formed double-stranded DNA, resulting in the precise and controlled replacement of a single-stranded sequence within the double helix. This process is primarily driven the binding of "input" strand to "toehold" region of double strand DNA,[11] which triggers a branch migration reaction involving a three-way or four-way exchange, and ultimately leads to the formation of a more stable DNA double helix within the system[12] (Scheme 1, DNA strand displacement reaction).

The rate of strand displacement is influenced by various factors, most notably is the toehold binding strength. In sufficiently dilute systems, strand displacement can be approximated as a second-order reaction, with the rate constant adjustable between 1 and 10^7 $M^{-1}s^{-1}$ by changing the toehold's sequence and length.[13] Therefore, DNA strand displacement reactions are highly specific and reversible, allowing for the precise programming of DNA sequences to carry out specific

[a] S. Bi, R. Yang, H. Ju, Y. Liu
State Key Laboratory of Analytical Chemistry for Life Science, School of Chemistry and Chemical Engineering, Nanjing University, Nanjing 210023, P. R. China
E-mail: yingliu@nju.edu.cn

[b] Y. Liu
Chemistry and Biomedicine Innovation Center, Nanjing University, Nanjing 210023, P. R. China

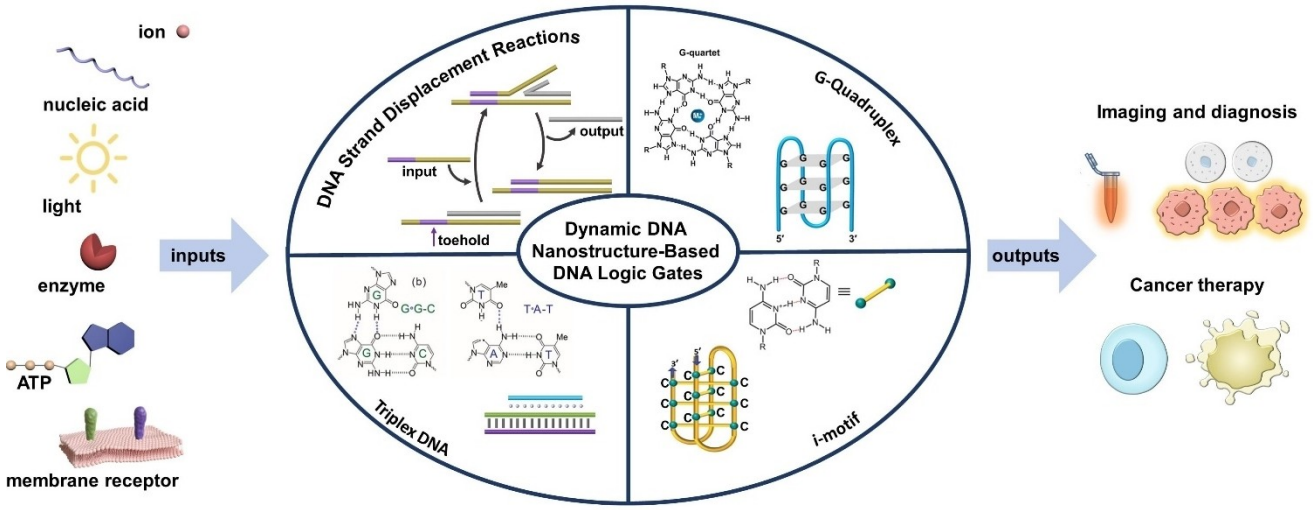

Scheme 1. Schematic illustration of dynamic DNA nanostructure-based DNA logic circuits responding to biomarkers of cancer cells or external stimuli for cancer diagnosis and treatment.

tasks, which make them appropriate for the complex processing and integration of biological signal.

2.2. Stimulus-Responsive DNA Structures

Beyond the classical Watson-Crick base pairing, DNA sequences can fold into stable non-classical structures, such as triple-stranded (triplex) and quadruple-stranded (G-quadruplex, i-motif) formations. These structures possess the ability to undergo reversible dynamic reconfigurations, offering a versatile means of controlling the structural transformations of corresponding nanomaterials and their properties.[14] Their unique structural and functional motifs significantly enrich the "toolbox" of dynamic DNA nanotechnology.

The incorporation of stimulus-responsive non-classical nucleic acids into DNA nanostructures presents a powerful strategy for modulating the spatial organization and hierarchical assembly of these structures. By responding to specific environmental triggers, these non-classical structures reconfigure dynamically, which is especially valuable in the design and construction of DNA logic gates and allows precise behaver and function controls.

Shiyi Bi obtained her Ph.D. degree in 2024 from Nanjing University. Her current research is mainly focused on engineering smart DNA structures for precise cancer treatment.

Ruowen Yang is a master's student at Nanjing university. Her research interests are in the design of nucleic acid probes and their applications in disease diagnosis and therapy.

Huangxian Ju is currently a professor at Nanjing University, the director of State Key Laboratory of Life Analytical Chemistry, a fellow of the International Electrochemical Society and a fellow of the Royal Society of Chemistry. His research interests focus on biosensing, bioimaging and clinical molecular diagnosis with the publications of 851 papers, 44 approved patents, 6 English books, 7 Chinese books, 20 chapters, and 8 editorials, preface or book reviews, which have 39,475 citations in SCI journals by other authors with an h-index of 102 (Google Scholar h-index 112).

Ying Liu is currently a professor at Nanjing University, China. She obtained her bachelor degree in 2004 and master degree in 2007 from Nanjing University, and Ph.D. degree in 2012 from University of California, Riverside. After completed postdoc training in University of California, Davis, she joined Nanjing University as an overseas high-level talent in 2015. She won the fund support of Chinese National Excellent Young Scholars in 2020. Her research interest focuses on the development of responsive nanomaterials for boimaging and therapy.

2.2.1. Triplex DNA

DNA triplexes are formed through the self-assembly of a DNA double helix with a third DNA strand via Hoogsteen or reverse Hoogsteen hydrogen bonding, with preferred base combinations including T·A–T, A·A–T, G·G–C, and CH^+·G–C (Scheme 1, Triplex DNA).[15] These triplex structures not only serve as recognition elements but also act as functional structural switches, generating signal output upon target recognition.[16] The incorporation of Hoogsteen interactions, as seen in DNA clamp-switch designs (Figure 1), significantly enhances binding affinity, contributing approximately 0.29 kcal/mol per base and providing ~3.3 kcal/mol in additional binding energy. This results in a roughly 200-fold increase in affinity compared to linear probes, along with improved specificity for perfectly matched sequences, offering a 1.2 kcal/mol increase in mismatch discrimination.[17]

Additionally, DNA triplexes are also involved in the catalytic functions of DNAzymes. For example, a Cu^{2+}-dependent DNAzyme executes its catalytic function by forming a DNA triplex with its substrate.[18] Specifically, the DNAzyme sequence include self-complementary regions that form a T·A–T/G·C–G triplex bridge with the DNAzyme substrate. Hybridization between the single-stranded domain of the DNAzyme and the complementary domain of the substrate facilitates the formation of the DNA triplex structure. In the presence of Cu^{2+}, selective cleavage occurs at the G–C base pairs of the substrate (Figure 2).

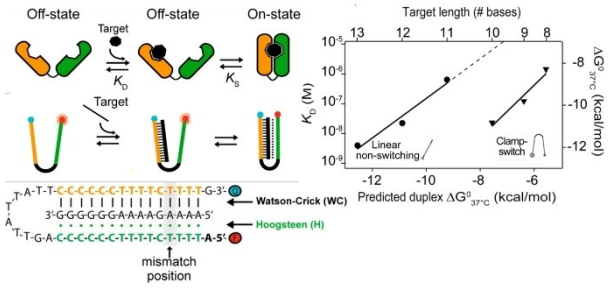

Figure 1. The experimentally derived affinities (and the equivalent free energies) of a clamp-switch and a linear non-switching probe using the same Watson-Crick recognition element versus target length (and the nearest neighbor model predicted binding energy). Adapted with permission from Ref. [17]. Copyright 2013, American Chemical Society.

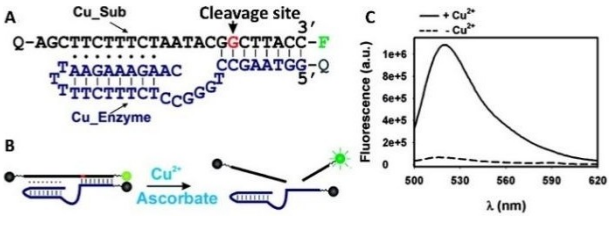

Figure 2. (A) The structure of the Cu^{2+}-dependent DNAzyme. (B) Schematic illustration of signal generation through Cu^{2+} responsive DNAzyme activation. (C) Fluorescence spectra of the sensor before and after Cu^{2+} addition. Adapted with permission from Ref. [18]. Copyright 2007, American Chemical Society.

The multifunctionality and enhanced thermodynamic properties make DNA triplexes critical components in the design of stimulus-responsive structures and DNA logic gates, where both high-affinity recognition and signal generation are essential.

2.2.2. G-Quadruplexes

G-quadruplexes are higher-order DNA structures formed by the stacking of two or more planar G-quartets through π-π interactions.[19] A G-quartet is a cyclic, planar structure composed of four guanines connected by Hoogsteen hydrogen bonds, creating a cavity with strong negative electrostatic potential. This cavity is stabilized by the coordination of central cations, such as K^+, NH^{4+}, or Na^+, which are essential for the integrity of the G-quadruplex.[20] The binding affinity of G-quadruplex structures is highly influenced by the presence of these cations, especially K^+, which stabilizes G-quartets in a cooperative manner. As shown in Table 1, shorter sequences like 21G and 22GT tend to stabilize only one K^+ ion, forming less stable, antiparallel 2-quartet structures, while longer sequences or those with flanking bases exhibit greater cooperativity, binding two K^+ ions with higher affinity. This sequential ion binding drives the transition to more stable G-quadruplex forms.[21]

G-quadruplexes can be formed from a single DNA strand or multiple DNA strands, and variations in strand orientation, length, and loop composition lead to diverse topological structures (Figure 3). Based on the orientation of the strands, G-quadruplexes can adopt parallel, antiparallel, or hybrid configurations.[22]

The reversible reconfiguration of G-quadruplexes is based on the ability of guanine-rich DNA strands to switch between G- quadruplex and classical DNA structures in response to appropriate trigger molecules. For example, Figure 4A illustrates the process where a complementary strand "C-fuel" opens a G-quadruplex "F21T" into a double-stranded structure. G-quadruplex could also be reformed by strand displacement reaction

Table 1. *K*D values at 20 °C of first and second K+ binding to G-quadruplex forming sequences (results of the fitting of the ESI-MS titration curves using DynaFit, with the errors from the fits).[21]

$DNA + K^+ \rightleftharpoons DNA \bullet K$ $\quad K_{D1} = [DNA][K^+]/[DNA \bullet K]$

$DNA \bullet K + K^+ \rightleftharpoons DNA \bullet 2K$ $\quad K_{D2} = [DNA \bullet K][K^+]/[DNA \bullet 2K]$

Name	Sequence	K_{D1} ($\times 10^{-6}$ M)	K_{D2} ($\times 10^{-6}$ M)
21G	$(GGG\ TTA)_3GGG$	18 ± 1	1660 ± 40
22GT	$(GGG\ TTA)_3GGG\ T$	22 ± 1	1050 ± 30
22CTA	$A\ (GGG\ CTA)_3GGG$	271 ± 6	6500 ± 600
22AG	$A\ (GGG\ TTA)_3GGG$	60 ± 4	1170 ± 70
23TAG	$TA\ (GGG\ TTA)_3\ GGG$	310 ± 30	170 ± 15
26TTA	$T_2A\ (GGGTTA)_3G_3TT$	1500 ± 100	190 ± 20
24TTG	$TT\ (GGG\ TTA)_3GGG\ A$	270 ± 40	10.4 ± 1.6
Pu24	$TGAG_3TG_4AG_3TG_4A_2G_2$	550 ± 100	3.8 ± 0.9

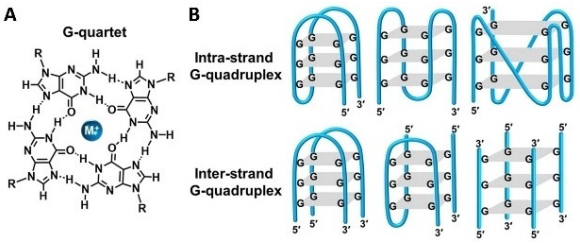

Figure 3. (A) The configuration of a metal-ion stabilized G-quartet. (B) Various structural motifs of G-quadruplexes. Adapted with permission from Ref. [22a]. Copyright 2022, Royal Society of Chemistry.

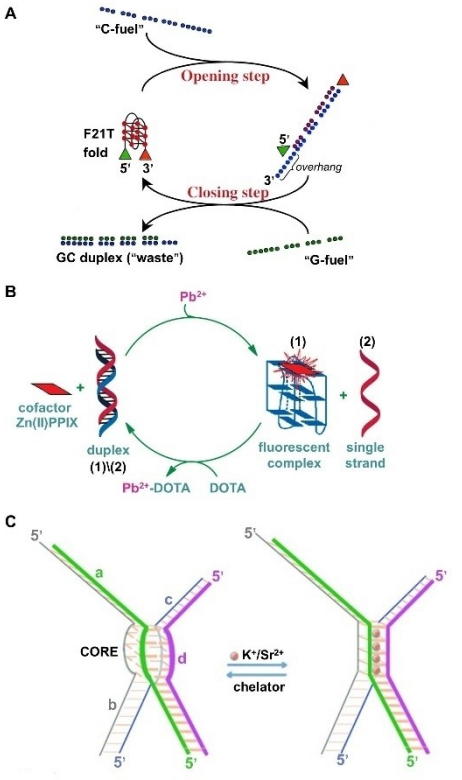

Figure 4. (A) Dynamic structural change between an intramolecular quadruplex (left) and a duplex (right) by using a "C-fuel" strand and a "G-fuel" strand. Adapted with permission from Ref. [23]. Copyright 2003, National Academy of Sciences. (B) Dynamic transformation of duplex nucleic acid structures and G-quadruplex in response to Pb^{2+} or DOTA stimuli. Adapted with permission from Ref. [24]. Copyright 2010, American Chemical Society. (C) Reversible structure changes between a four-armed DNA duplex with a guanosine-rich core (left) and a stable G-quadruplex structure (right). Adapted with permission from Ref. [25]. Copyright 2014, WILEY-VCH Verlag GmbH & Co. KGaA, Weinheim.

between the as-obtained double strand with a counter strand "G-fuel".[23] The formation and dissociation of the G-quadruplex are monitored using a fluorophore/quencher pair as an imaging probe. Additionally, Pb^{2+} can induce the separation of a double-stranded structure (1)/(2) to form a Pb^{2+}-stabilized G-quadruplex (1), which subsequently binds to cofactor Zn(II)PPIX to generate fluorescence. The G-quadruplex can then be reverted back to a double-stranded structure by chelating Pb^{2+} ions with 1,4,7,10-tetraazacyclododecane-1,4,7,10-tetraacetic acid (DOTA) as a chelating agent (Figure 4B).[24] Similarly, in the presence of K^+ or Sr^{2+}, four G-rich subunits (a-d) self-assemble into a G-quadruplex structure, which can then be reconfigured by separating the G-quadruplex from the ions using a crown ether-type chelating agent (Figure 4C).[25]

Additionally, certain aptamers can form G-quadruplex/protein complexes upon binding to their target proteins, which subsequently inhibits the catalytic function of the proteins. These G-quadruplex/protein complexes are considered multifunctional therapeutic targets, for example, in inhibiting thrombin in the coagulation pathway or suppressing the transcription of oncogenes such as c-MYC.[26] Based on this principle, carriers loaded with drug/dye can be encapsulated with aptamers to create "smart" dynamic gates. These gates are unlocked in specific cell types when the overexpressed protein biomarkers, such as vascular endothelial growth factor (VEGF) and thrombin, induce the aptamers to convert into G-quadruplexes. This transformation enables the dynamic response for chemotherapeutic or photodynamic therapy applications (Figure 5).[27]

2.2.3. i-motif

The i-motif is a type of four-stranded nucleic acid formed by the folding of cytosine-rich DNA sequences under acidic conditions.[28] Its structure consists of two parallel double-stranded motifs, which are held together in an antiparallel arrangement by embedded hemi-protonated cytosine-cytosine (C^+-C) base pairs (Scheme 1, i-motif). The protonation of cytosines allows i-motif to maintain structural integrity across a relatively broad pH range. The folding process involves two kinetic phases (Figure 6): an initial fast folding step leads to a less stable conformation (3'E), followed by a slower transition to the thermodynamically favored conformation (5'E). The 3'E conformation forms more rapidly (with rate constants between 1.66 and 2.90 min^{-1}), while the 5'E conformation, though slower to form (0.21–0.89 min^{-1}), is more stable at equilibrium.[29] These properties enable i-motifs to respond rapidly and reversibly to pH changes, making them widely used in the dynamic regulation of nanostructures.[30]

Table 2 summarized the dynamic DNA nanostructures that have been used in DNA logic circuits.

Figure 5. Schematic illustration of G-quadruplex conformational change in response to vascular endothelial growth factor, promoting the release of drugs/dyes from NMOF. Adapted with permission from Ref. [27]. Copyright 2021, Royal Society of Chemistry.

Table 2. Dynamic DNA nanostructures used in DNA logic circuits.

Probe motif	Target	Mechanism	Biomedical applications	Refs.
DNA duplex	DNA strands/ RNA strands	Input strand triggers strand displacement for signals release or further amplification	Molecular computing; imaging and diagnosis; smart therapy	[37, 38, 44]
i-motif sequence	pH	pH promotes the formation or disruption of i-motif structures to release signals or trigger subsequent reactions		[34, 37]
G-quadruplex sequence/ partial aptamer	Metal ions/ small molecules/ protein	target triggers the formation or disruption of G-quadruplex structures to release signals or active downstream reactions		[33, 34]
Triplex DNA sequence/ partial DNAzyme	pH/metal ions	target promotes the formation or disruption of triplex DNA structures to release signals or trigger subsequent reactions.		[18]

3. Biological Application of Dynamic DNA Nanostructure-Based Logic Devices

3.1. Imaging and Diagnosis

Dynamic DNA nanostructure-based logic devices offer versatile tools for simultaneously detecting multiple molecular targets in tumor tissue, significantly improving cancer imaging and diagnostics. These devices are particularly effective at detecting small molecules, nucleic acids, and protein biomarkers that related in cancer development and progression.

3.1.1. Tumor Microenvironment Powered DNA Logic Circuits

The tumor microenvironment (TME) is a complex and dynamic network of cells and extracellular matrix surrounded by signaling molecules.[31] Compared to normal tissues, tumor tissues exhibit abnormal metabolic properties, including lower pH, elevated adenosine triphosphate (ATP) levels, increased concentrations of glutathione (GSH) and potassium (K^+).[32] These tumor microenvironment difference could be used as external stimuli to power DNA logic circuits for accurate distinguishment of cancer cells with normal cells.

Leveraging these differences in the TME, Gong et al. developed a YES-AND logic gate for differentiating normal cells from cancer cells by detecting the elevated levels of K^+ and ATP (Figure 7A).[33] The DNA nanoassemblies were only activated when both inputs (K^+ and ATP) were present, triggering a fluorescence resonance energy transfer (FRET) signal. This multi-input detection mechanism significantly enhanced the specificity of cancer cell identification, ensuring that the response occurred exclusively in the presence of cancer-specific extracellular conditions. Similarly, Peng et al. constructed extracellular H^+ and K^+-responsive framework nucleic acid (FNA) logic nanosensors for in situ bioimaging, further demonstrating the potential of such systems in accurately distinguishing cancer cells from normal cells (Figure 7B).[34]

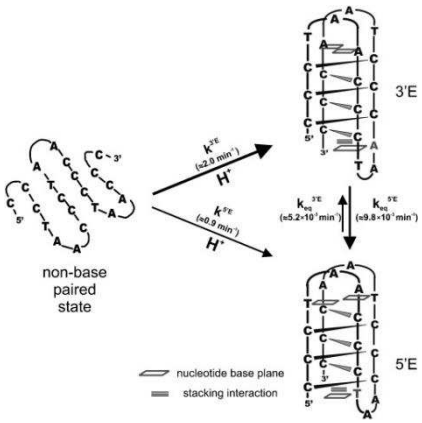

Figure 6. Model of the folding pathway of the DNA i-motif. After a pH jump from pH 9–6, major (5'E) and minor (3'E) conformations are formed. Adapted with permission from Ref. [29]. Copyright 2012, WILEY-VCH Verlag GmbH & Co. KGaA, Weinheim.

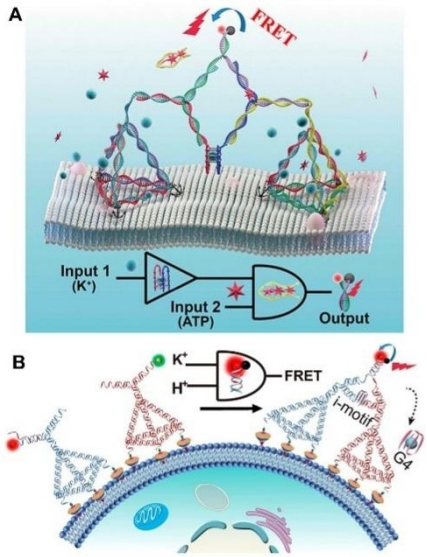

Figure 7. (A) Schematic illustration of DNA logic circuit controlled by extracellular stimuli (K^+ and ATP) on the cell surface. Adapted with permission from Ref. [33]. Copyright 2022, American Chemical Society. (B) A dimerized AND-gated FNA logic sensor for extracellular H^+ and K^+ sensing and imaging. Adapted with permission from Ref. [34]. Copyright 2020, American Chemical Society.

3.1.2. Nucleic Acid Markers Powered DNA Logic Circuits

Messenger RNAs (mRNAs) are crucial in conveying genetic information required for protein synthesis.[35] Alterations in mRNA metabolism are hallmarks of cancer, and their expression levels vary across different stages of tumor progression. Therefore, numerous tumor-associated mRNAs are commonly employed as specific biomarkers to assess tumor cell invasion.[36]

Wang et al. reported a DNA-based functional logic circuit integrated with framed nucleic acid (FNA) nanocarriers for imaging intracellular mRNA (Figure 8A).[37] They used protons and ATP, typically present at elevated levels in tumor cells, as dual input signals to activate OR-AND and AND-AND logic gates. The FNA nanocarrier included embedded logic control units, i-motif and ATP aptamer (ABA27). The OR-AND gate was activated by ATP or H^+, whereas AND-AND gate required both ATP and H^+ for activation. Upon activation, these gates controlled the release of antisense oligonucleotides (ASOs) from FNA nanocarrier, which were subsequently recognized by target TK1 mRNA and correspondingly recovered Cy5 fluorescence for self-quenched FNA. The system responded to mRNA expression level change with identification specificity and quantifying accuracy, making it useful for early-stage cancer detection. To achieve precise cancer cell discrimination, Zhong et al. designed a DNA octahedron-based AND logic gate fluorescence nanoprobe that simultaneously detect dual tumor-related mRNAs (Figure 7B).[38] In response to target mRNAs, the probe could generate respective fluorescent signals, which significantly enhanced detection specificity and sensitivity. Similarly, another study designed a DNA windmill probe that integrates multiplexed mRNA detection with logic gates to accurately discriminate different cell types.[39] This multi-input activation mechanism ensured cell type specific activation of nanoprobe, providing crucial support for precise cancer diagnosis.

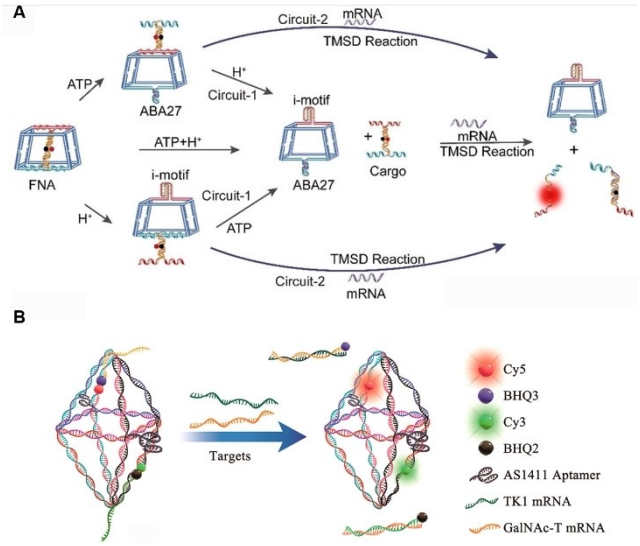

Figure 8. (A) The OR-AND and AND-AND logic gates for imaging intracellular mRNA. Adapted with permission from Ref. [37]. Copyright 2020, WILEY-VCH Verlag GmbH & Co. KGaA, Weinheim. (B) A DNA octahedron-based AND logic gate fluorescent nanoprobe activated by dual tumor-associated mRNA. Adapted with permission from Ref. [38]. Copyright 2018, American Chemical Society.

MicroRNA (miRNA) is a class of small, non-coding single-stranded RNA molecules, typically 20–24 nucleotides in length, that are encoded by endogenous genes.[40] These molecules function as key post-transcriptional regulators of gene expression.[41] Many miRNAs demonstrate high expression levels in cancer cells and tissues, making them valuable biomarkers for tumor diagnosis and prognosis.[42]

Zhao et al. designed a DNA logic gate nanodevice with high spatial and temporal accuracy for imaging miRNAs in living cells and animals (Figure 7A).[43] The nanodevice was controlled by near-infrared (NIR) light as the first input. Specifically, the nanodevice was constructed using UV-sensitive DNA molecular beacons and upconversion nanoparticles (UCNPs), UCNPs could absorb NIR light and emit UV light to activate the beacon in situ. UCNPs coated with a cationic polymer (polylysine) as carriers for DNA molecular beacons also facilitate cellular uptake, ensuring that the nanodevices effectively reach the target cells and maximize their imaging capabilities. This design allowed the nanodevices to remain inactive until exposed to NIR light, allowing precise control of the timing and location of miRNA imaging. Upon activation, the DNA logic gate within the nanodevice bound to the target miRNA, generating a fluorescent signal for imaging. The system not only provided highly specific and sensitive miRNA detection, but also enabled real-time monitoring of miRNA levels in living cells, which was critical for tracking cancer progression and treatment response. Integrating miRNA controllers into DNA logic gates is crucial for precise cell subtype identification at the molecular level.

However, considering cancer biomarker miRNA can also be expressed by normal cells sometimes, it requires the participations of multiple miRNAs to provide more accurate differentiation of cancer cells. Yang et al. constructed a DNA logic circuit to identify multiple cancer cell subtypes through bispecific miRNA recognition (Figure 9B).[44] This circuit featured a DNA nanohexahedron framework equipped with three recognition modules for miR-21, miR-155, and miR-373 respectively, with three reporting modules FAM, Cy3 and Cy5, creating three "AND" logic gates. The DNA nanohexahedral framework facilitates the delivery of DNA into cells. Simultaneous existence of two miRNAs activated "AND" logic gate, which could be used to distinguish between the three cell subtypes. This system effectively distinguished between cancer cells (A549 and MCF-7) and normal cells (NHDF), as well as differentiated various cancer cell types. Recent studies have shown that the concentrations of various microRNAs in serum can serve as valuable biomarkers for cancer diagnosis. Zhang et al. developed a DNA molecular computation platform to analyze miRNA profiles in clinical serum samples.[45] Their approach enabled rapid and precise cancer diagnosis, achieving an accuracy of 86.4% with serum samples from 22 healthy individuals and 14 lung cancer patients.

Elevated or altered levels of specific circular RNA (circRNA) in tumor tissues or blood can indicate the presence and progression of cancer, aiding in early diagnosis and personalized treatment strategies.[46] In addition to cancer subtype

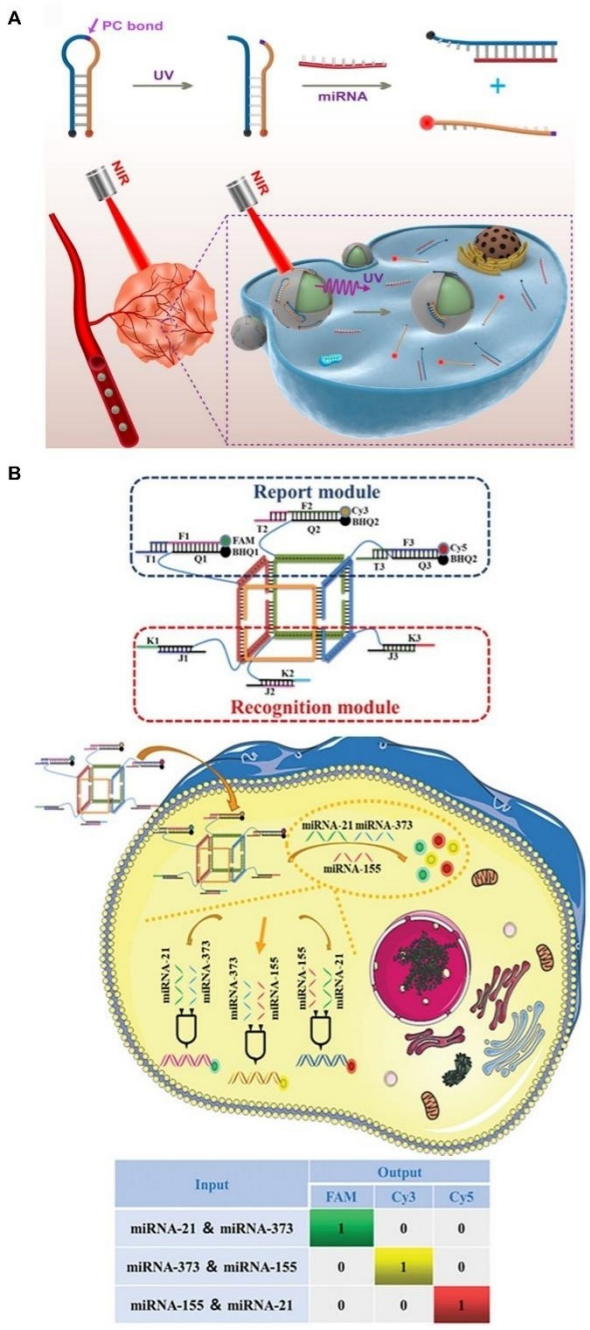

Figure 9. (A) A DNA logic gate nanodevice with NIR light controlled miRNA imaging and sensing. Adapted with permission from Ref. [43]. Copyright 2019, American Chemical Society. (B) A three "AND" logic gates formed by DNA nano-hexahedron framework with extending three recognition modules and three reporting modules. It was used for cell subtype discrimination by detecting multiple miRNAs, with the corresponding relation between target and fluorescent group illustrated at the bottom. Adapted with permission from Ref. [44]. Copyright 2021, WILEY-VCH Verlag GmbH & Co. KGaA, Weinheim.

discrimination, logic operation system was also used for distinguish circRNA and linear RNA. Bai et al. explored series toehold-mediated strand displacement (STMSD) in three strand displacement modes which relied on varying secondary structures.[47]

3.1.3. Membrane Receptor Powered DNA Logic Circuits

The cell membrane, serving as the boundary of the cell, could effectively distinguish normal cells and tumor cells due to the expression of specific membrane receptors.[48]

Peng et al. engineered an aptamer-based 3D DNA-logic gate triangular prism (TP) nanomachine for bispecific recognition and computation on the surfaces of cancer cells to distinguish cancer cell types (Figure 10A).[49] This structure integrated two DNA aptamers, sgc8c and sgc4f, which specifically targeted overexpressed protein receptors, that acted as logic gates, capable of performing Boolean logic operations, specifically the "AND" operation. When the TP nanomachine encountered both cell membrane receptors, it caused displacement and release of the complementary strand, which recovered fluorescence for the reporter region. The signal indicated specific cancer cell type, CCR-CEM cells, which distinguished it from other cell types that only had single membrane receptor expression, such as Ramos cells. Similarly, Song et al. introduced an architecture with multiple interacting nodes driven by cell membrane receptors (Figure 10B).[50] The circuit was activated only when all targeted receptors were present on the cancer cell membrane. The flexible addressing mechanism allowed easy reprogramming of nodes to target various cancer cell membrane receptors, offering a promising approach for cancer cell detection. By integrating proximity induced hybridization reaction with DNA cascade reaction, Chang et al. designed a signal amplification strategy for tumor cell membranes protein identification (Figure 10C).[51] This method could distinguish four similar tumor cells in a single step, providing an effective tool for accurate tumor cell typing and analysis.

Tumor-derived extracellular vesicles (tEVs) are essential for cancer initiation and progression, making them valuable for non-invasive diagnosis.[52] However, the detection of tEVs is complicated by their similarity to non-tumor EVs, which often share similar sizes and membrane protein markers with only subtle differences in expression levels.

Li et al. developed a thermophoresis-mediated DNA computation device for the molecular identification of tEVs (Figure 10D).[53] This device employed aptamers targeting cancer-specific proteins, epithelial cell adhesion molecule (EpCAM) and human epidermal growth factor receptor 2 (HER2). The DNA logic gate in the device was activated in the presence of both proteins, then triggered a toehold-initiated hybridization chain reaction (HCR) for signal amplification. To enhance sensitivity, tEVs were captured by CD63-aptamer-modified microbeads and enriched through thermophoresis. This system accurately distinguished breast cancer patients from healthy donors with 97% accuracy, which matched well with traditional biopsy results, making it a promising tool for non-invasive cancer diagnostics.

3.1.4. Protein/Enzyme Powered DNA Logic Circuits

Protein-level biomarkers are also of significant value in cancer diagnosis. Base excision repair (BER) is a key DNA repair

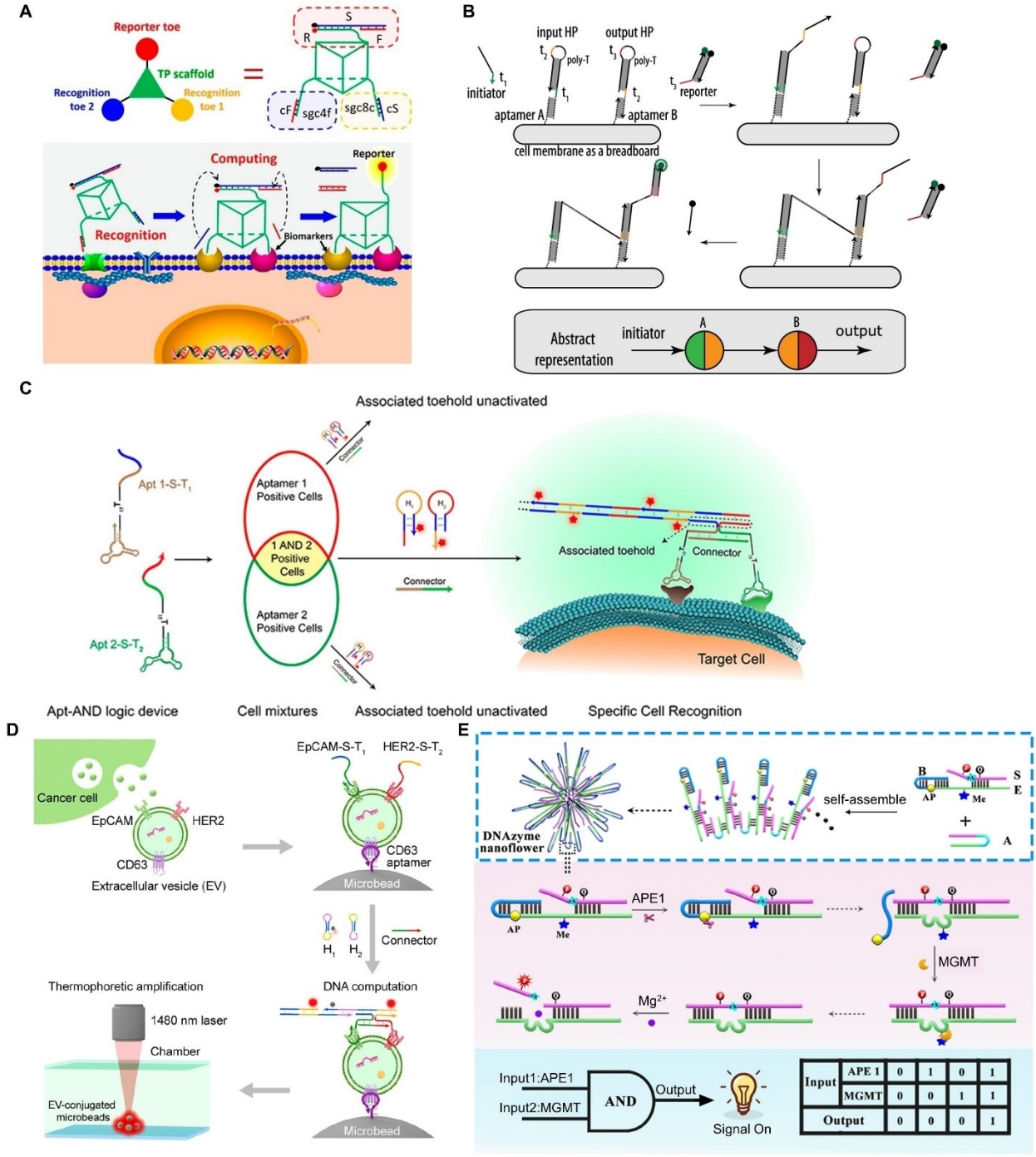

Figure 10. (A) A DNA-logic gate TP nanomachine for bispecific receptor recognition and computation to distinguish cancer cell types. Adapted with permission from Ref. [49]. Copyright 2018, American Chemical Society. (B) Two-layer linear cascade with multiple interacting nodes driven by cell membrane receptors. Adapted with permission from Ref. [50]. Copyright 2019, American Chemical Society. (C) Multi-aptamer-based AND logic device for cell identification and isolation. Adapted with permission from Ref. [51]. Copyright 2019, American Chemical Society. (D) Thermophoresis-mediated DNA computation device on EV membranes. Adapted with permission from Ref. [53]. Copyright 2021, American Chemical Society. (E) DNAzyme nanoflower simultaneously processed by APE1 and MGMT to produce a specific fluorescent signal. Adapted with permission from Ref. [55]. Copyright 2024, American Chemical Society.

mechanism in mammalian cells, which includes apurinic/apyrimidinic endonuclease 1 (APE1) removing apurinic/apyrimidinic (AP) sites and O6-methylguanine methyltransferase (MGMT) transferring alkyl adducts at O6-methylguanine (O6-MeG).[54] Therefore, monitoring the activity of these repair enzymes supports early cancer diagnosis.

Zeng et al. designed an AND logic gate DNAzyme nanoflower to differentiate cancer cells based on the activity of two DNA repair enzymes (Figure 10E).[55] The DNAzyme nanoflower was constructed by self-assembling DNA duplexes modified with AP sites and O6-methylguanine lesions. APE1 recognized and cleaved AP sites on the DNA nanoflower, partially restored

DNAzyme's structure. MGMT then repaired the O6-methylguanine lesions, fully reactivated DNAzyme and recovered fluorescent signal. This AND gate mechanism ensured that only cancer cells with elevated levels of both APE1 and MGMT were identified, minimized false positives and achieved precise identification of cancer cell types. This was crucial for distinguishing different cancer cell types and stages, improving the accuracy of early cancer diagnosis and allowing for more personalized treatment strategies.

Telomerase (TE) is an enzyme that maintains telomere length by adding guanine-rich repeats. Telomerase is closely associated with cellular immortalization and tumorigenesis, making it an efficient biomarker for early cancer diagnosis.[56]

Fan et al. designed an AND logic gate to differentiate cancer cells by monitoring TE and APE1 activities (Figure 11).[57] The DNA reporter contained TE responsive region and APE1 responsive region. TE initiated DNA elongation, while APE1 mediated specific cleavage of DNA backbone. The DNA structure only unfolded and recovered fluorescence with the appearance of both TE and APE1. This approach provided a powerful tool for precise cancer diagnostics and disease progression monitoring. Similarly, Shi et al. used TE and miR-21 as inputs for cancer cell identification with reduced false positives.[58]

3.2. Precise Cancer therapy

3.2.1. Gene Therapy

Small interfering RNA (siRNA) technology, which selectively silences gene expression and inhibits protein synthesis, is emerging as a promising method for cancer treatment.[59] However, developing a cell-specific and efficient delivery system that minimizes nonspecific binding and limits off-target effects in non-target cells is crucial.

Ren et al. programmed a dual-parameter-controlled DNA logic platform for delivering siRNA exclusively to specific cancer cell subtypes (Figure 12A).[60] The DNA logic gate system used two different aptamers (sgc4f and sgc8c) as inputs. Precise siRNA delivery with cell sub-type discrimination was achieved upon sequential reactions with two cell membrane proteins. Jiang et al. utilized a miRNA-responsive AND gate to trigger the in situ generation of siRNA for targeted gene therapy in cervical carcinoma (Figure 12B).[61] Upon binding to miR-21, the system initiated a catalytic hairpin assembly (CHA) reaction through a series of AND logic gates, leading to the self-assembly of DNA nanowheels (DNWs) and the in situ generation of VEGF-specific siRNA. The siRNA was then processed by endogenous Dicer enzymes, resulting in the downregulation of VEGF mRNA and protein, effectively suppressed tumor growth.

3.2.2. Chemotherapy

Precise delivery of chemotherapy drugs can avoid side-effect and nonspecific toxicity, which is crucial for targeted cancer treatment. Zhou et al. developed mesoporous silica nanoparticles (MSNs) functionalized with DNA strands, which were controlled by AND logic gate mechanism (Figure 13A).[62] The MSNs were capped with DNA strands intercalated with acridinamine, a drug molecule which also stabilized the structure of DNA gate. The system integrated various stimuli into an AND

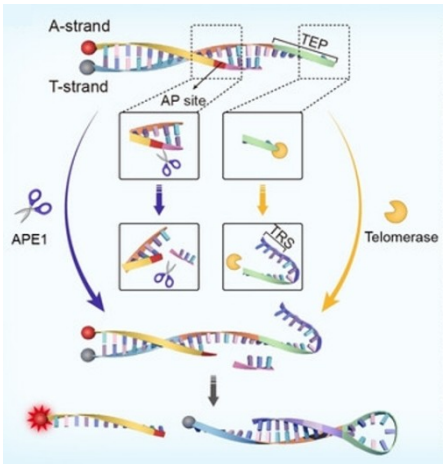

Figure 11. An AND DNA logic gate to differentiate cancer cells by monitoring TE and APE1 activities. Adapted with permission from Ref. [57]. Copyright 2021, WILEY-VCH Verlag GmbH & Co. KGaA, Weinheim.

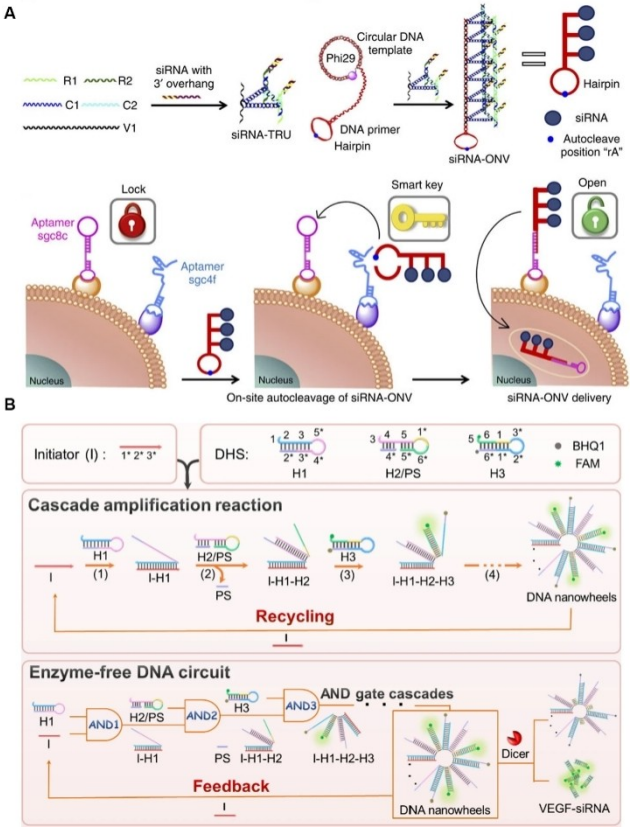

Figure 12. (A) A dual-parameter-controlled DNA logic platform for cell-subtype-specific siRNA delivery and gene silencing. Adapted with permission from Ref. [60]. Copyright 2021, Nature. (B) A miRNA-responsive AND gate for triggering in situ generation of siRNA. Adapted with permission from Ref. [61]. Copyright 2021, Springer Link.

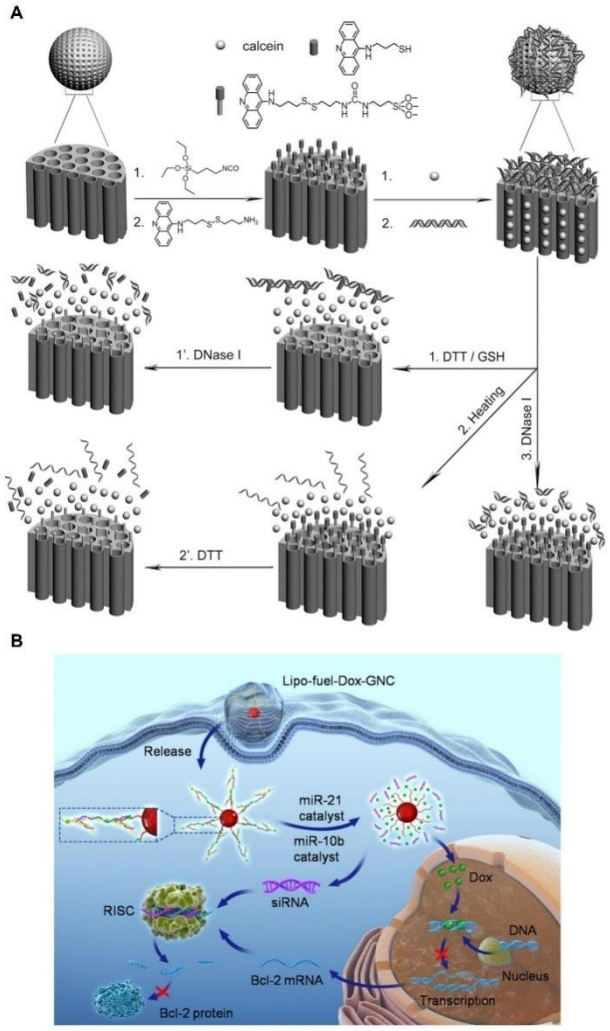

Figure 13. (A) DNA-gated mesoporous silica nanoparticles (MSNs) and logic-controlled release of loading cargoes. Adapted with permission from Ref. [62]. Copyright 2014, WILEY-VCH Verlag GmbH & Co. KGaA, Weinheim. (B) Schematic illustration of Dox release by dual miRNA programming. Adapted with permission from Ref. [63]. Copyright 2020, American Chemical Society.

logic gate, such as disulfide-reducing agents, elevated temperature, and DNase I. When the appropriate stimuli were present, the DNA gate was disrupted and released the encapsulated doxorubicin (DOX) into tumor cells. This multi-input design effectively enhanced the specificity of the delivery system. Similarly, Yue et al. utilized dual miRNA inputs-based AND logic gates to trigger DOX release, thereby enabled a combination of targeted chemotherapy and gene therapy (Figure 13B).[63]

3.2.3. Photodynamic Therapy

Photodynamic Therapy (PDT) relies on photosensitizers which produce reactive oxygen species (ROS) upon light excitation to damage and destroy cells or tissues, leading to therapeutic effects.[64] However, photosensitizers could not differentiate normal and tumor cells, therefore would cause non-specific damage. To address this, DNA logic circuits have been utilized to develop precise PDT strategies with specific cancer cells targeting capability.

Zhang et al. reported a transmembrane DNA logic gate for precise PDT in solid tumors (Figure 14A).[65] The nanomachine consisted of multi-shell upconversion nanoparticles (UCNPs) and DNA frameworks. The two inputs included a cancer cell membrane overexpressed receptor PTK7 (input 1) and intracellular miRNA-21 (input 2). The DNA nanomachine bound to input 1 at the cell membrane, which exposed the recognition site for miRNA-21 and resulted in endocytosis of DNA nanomachine. miRNA-21, as input 2, completed the "AND" logic gate operation by activating photosensitizer Rose Bengal (RB) to generate ROS. This ensured that ROS generation was confined to the targeted cancer cells, minimizing damage to surrounding healthy cells and enhancing treatment precision. Compared to saline-treated mice, those treated with the DNA nanomachine showed minimal changes in hematological parameters and serum IL-1β levels, further confirming the nanomachine's safety and immunocompatibility.

3.2.4. Chemodynamic Therapy

Unlike PDT, which relies on light to activate photosensitizers, chemodynamic therapy (CDT) uses chemical agents to generate reactive oxygen species (ROS) through chemical reactions.[66] Similar to PDT, CDT also faces the challenge of nonspecific toxicity and damage to healthy tissues.

Wang et al. combined a dual-response DNAzyme (DR-DNAzyme) logic system with a prussian blue (PB) analog metal-organic framework (MOF) to construct an intelligent nanomachine (Figure 14B).[67] The DR-DNAzyme logic gate was activated by two inputs, miR-21 and H_2O_2. The activated DR-DNAzyme could cleave catalase mRNA, which inhibited catalase activity and subsequently caused H_2O_2 accumulation. This generated a positive feedback loop and allowed continuous H_2O_2 production in cancer cells. In contrast, the DR-DNAzyme remained inactive in normal cells due to the low levels of miR-21 and H_2O_2. The effect of the nanomachine on tumor growth was evaluated in female nude mice with MCF-7 tumors. Tumor reduction was significant in both the DR-DNAzyme@PBA and DNAzyme@PBA groups. However, mice in the DNAzyme@PBA group experienced noticeable weight loss and liver damage, likely due to non-selective targeting of normal cells, limiting its potential for practical use. In contrast, the DR-DNAzyme@PBA nanomachine showed no significant side effects, thanks to its cancer cell-specific recognition mechanism.

3.2.5. Cell Membrane Receptor Clustering Manipulation

Cell membrane receptors bridge and facilitate communication between the internal and external environments of cells. Manipulating these receptors clustering can alter signal transduction pathways and redefine cell functions, providing a promising tool to control cell-environment interactions.[68] The

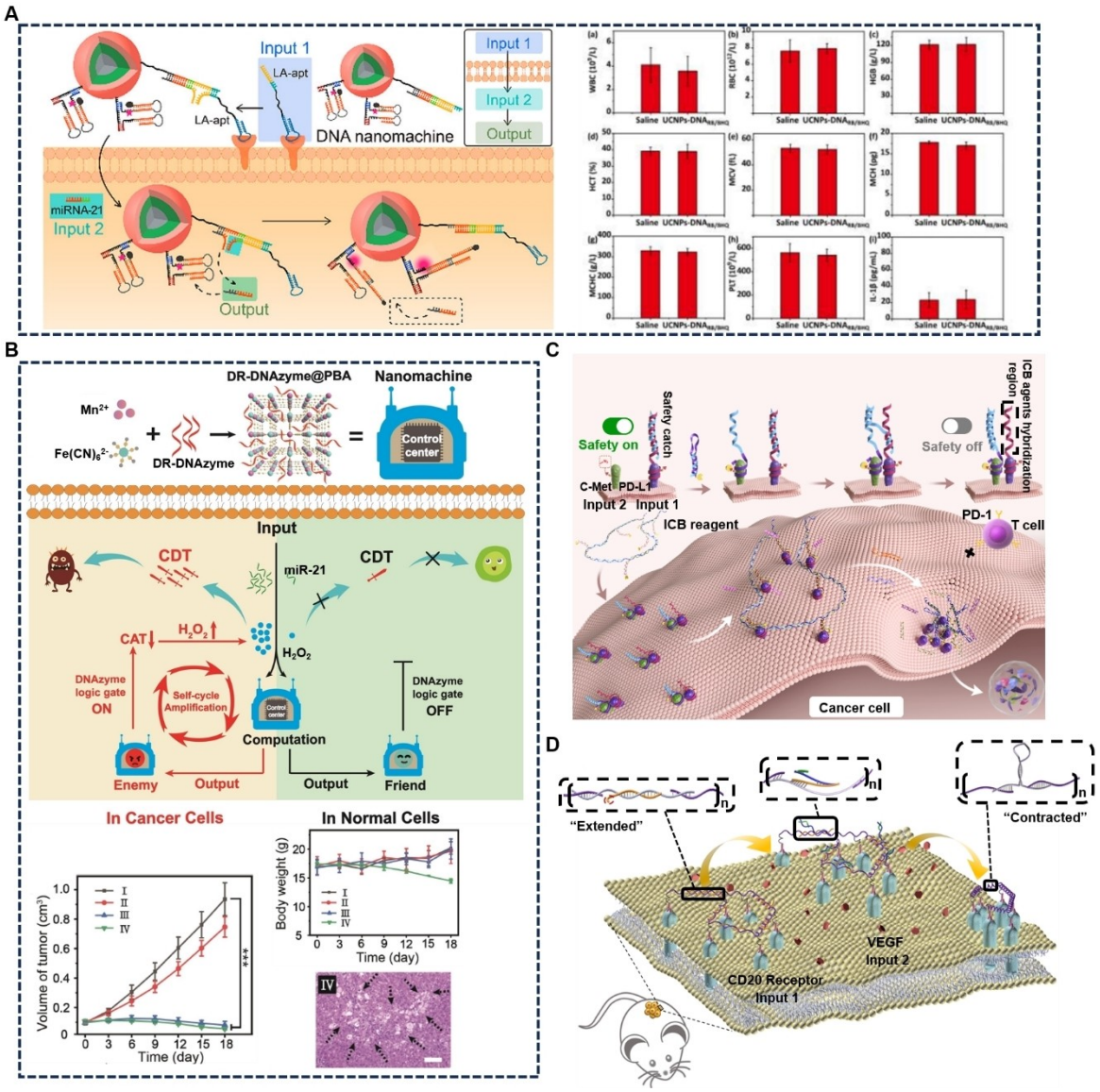

Figure 14. (A) A transmembrane DNA logic gate for precise PDT in solid tumors. Blood analysis results including (a) WBC, (b) RBC, (c) HGB, (d) HCT, (e) MCV, (f) MCH, (g) MCHC, (h) PLT and (i) IL-1β of mice injected with saline and multi-shell UCNPs-DNA$_{RB/BHQ}$. Adapted with permission from Ref. [65]. Copyright 2021, American Chemical Society. (B) An intelligent nanomachine guided by a DNAzyme logic system for precise CDT. Tumor volumes, mouse weight, and liver H&E staining were assessed following four treatments: I) PBS, II) cDNA@PBA, III) DR-DNAzyme@PBA, and IV) DNAzyme@PBA. Adapted with permission from Ref. [67]. Copyright 2022, WILEY-VCH Verlag GmbH & Co. KGaA, Weinheim. (C) A safety catch controlled by DNA logic gate for selectively degrading PD–L1 on tumor cells. Adapted with permission from Ref. [70]. Copyright 2024, WILEY-VCH Verlag GmbH & Co. KGaA, Weinheim. (D) A DNA nanostring for selectively manipulating CD20 receptor clustering driven by tumor secretion VEGF. Adapted with permission from Ref. [71]. Copyright 2023, American Chemical Society.

selective reprogramming of tumor cells and precise manipulation of their surface receptor distribution at the nanoscale are vital for promoting treatment targeting, minimizing side effects, and advancing more effective therapies.

Non-selective immune checkpoint inhibition can cause the immune system to attack both normal and tumor cells, leading to potentially fatal immune-related adverse events (irAEs).[69] To address this, Bi et al. developed a DNA logic gate strategy for selectively degrading PD–L1 on tumor cells (Figure 14C).[70] They assembled a double-stranded DNA "safety catch" on PD–L1, using PD–L1 as input 1 and the overexpressed c-Met on cancer cells as input 2 to control the accessibility of PD–L1 to immune checkpoint blockade (ICB) agents. In non-cancer cells, due to the absence of input 2 (c-Met), the safety catch remained in "safety on" state, which prevented ICB agents binding and protected normal cells. In cancer cells, however, input 2 (c-Met) induced the safety catch on input 1 (PD–L1) to expose its hybridization region, and subsequently allowed ICB agents to bind. The ICB agent, a retractable DNA nanostring, then contracted on cell membrane to cause PD–L1 aggregation and lysosomal degradation. This strategy showed high selectivity and potent immune-blocking effects on cancer cells *in vitro and in vivo*, reduced irAEs and showed promise for precision immunotherapy in mice. In another study, they utilized CD20

and cell-secreted VEGF as two inputs to selectively manipulate CD20 receptor clustering in tumor cells, which precisely induced cancer cell apoptosis by triggering calcium ion influx (Figure 14D).[71] On the contrary, the activity of B cells, which also express CD20 on cell membrane but in lack of VEGF secretion, was not affected.

3.2.6. Dynamic Cell-Cell Interactions Control

Cell-cell interactions are critical for various cellular behaviors such as epithelial cell closure, tissue elongation, and tumor progression.[72] Disruption of these interactions (e.g., specificity and strength) can lead to biological dysfunctions such as metabolic disorders as well as autoimmune diseases and cancer.[73] Thus, precise regulation of cell-cell interactions is essential for studying multicellular behavior, which provides new ways to manipulate cellular processes and develop cell-based therapies.

Tang et al. discusses the use of DNA logic gates for precise control of cell-cell interactions in cancer immunotherapy by designing a chimeric conjugate of antibodies and programmable DNA nanoassembly (Figure 15).[74] The chimeric platform involves a DNA-protein conjugate with two functional arms. One arm uses aptamer-based DNA nanoassembly for precise recognition of cancer cells, while the other arm uses a T-cell engaging antibody that recruits and activates T cells through CD3-binding. The DNA nanoassembly circuits are programmed to perform high-order logic operations (such as AND gates) that require the simultaneous presence of multiple cancer antigens. This ensures that T cells are activated only when cancer cells exhibit a specific antigen profile, which reduces off-target effects on healthy tissues. Furthermore, the valency of antigen-targeting aptamers is precisely controlled using DNA dynamic nanoassembly, allowing fine-tuning of the binding strength (avidity) between T cells and cancer cells. This study showcases the potential of using DNA logic gates in conjunction with T-cell therapy to achieve precise control over cell-cell interactions, significantly improving the specificity and efficacy of cancer immunotherapy.

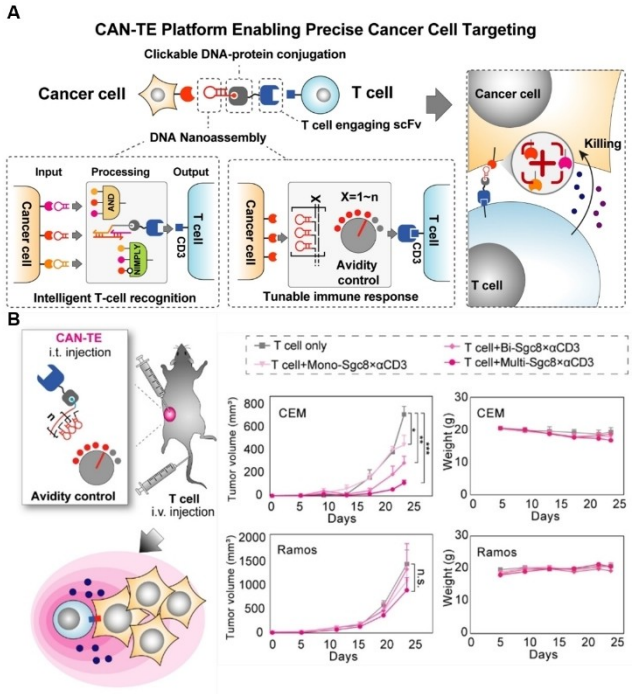

Figure 15. A chimeric conjugate of antibody and programmable DNA nanoassembly for precise control of cell-cell interactions. Adapted with permission from Ref. [74]. Copyright 2022, WILEY-VCH Verlag GmbH & Co. KGaA, Weinheim.

3. Summary and Outlook

By utilizing the programmability and specific recognition capabilities of DNA, dynamic DNA nanostructure-based DNA logic gates have shown great potential in precise cancer diagnosis and treatment. In this review, various examples of DNA logic circuit-based diagnosis and therapy strategies were discussed in detail. However, several challenges remain for clinical transition, including the structure stability in complex biological systems, circuit leakage during operation, and accurate spatiotemporal control.

Recent advances in artificial intelligence (AI) are helping to address these challenges. AI technologies, such as machine learning and optimization algorithms, have improved DNA logic gate design by optimizing sequences, predicting reactions, and enabling precise multi-input operations, reducing signal leakage. AI has also advanced smart diagnostics by aiding targeted probe design and adaptive networks, enhancing specificity, sensitivity, and response in detecting cancer biomarkers. Additionally, AI-driven systems integrate diagnostic and therapeutic functions, paving the way for personalized therapies and immunotherapy.

Future research should focus on enhancing the stability of DNA logic circuits in physiological environments through specific DNA modifications, while expanding their detection targets and therapeutic functions. These efforts will contribute to the development of next-generation biotechnologies, including cancer stem cell targeting and smart cancer treatment strategies, ultimately improving the reliability and clinical transition of DNA logic-based approaches.

Acknowledgements

We gratefully acknowledge the National Natural Science Foundation of China (22022405, 22374073, 21974064), Natural Science Foundation of Jiangsu Province for Distinguished Young Scholars (BK20200010), State Key Laboratory of Analytical Chemistry for Life Science (5431ZZXM2204, 5431ZZXM2307).

Conflict of Interests

The authors declare no conflict of interest.

Keywords: dynamic DNA nanostructure · DNA logic gates · stimuli-responsive · imaging and diagnosis · cancer therapy

[1] a) M. A. Moses, H. Brem, R. Langer, *Cancer Cell* **2003**, *4*, 337; b) G. Tiwari, R. Tiwari, B. Sriwastawa, L. Bhati, S. Pandey, P. Pandey, S. K. Bannerjee, *Int. J. Pharm. Investig.* **2012**, *2*, 2; c) C. Lindley, J. S. McCune, T. E. Thomason, D. Lauder, A. Sauls, S. Adkins, W. T. Sawyer, *Cancer Pract.* **1999**, *7*, 59.
[2] a) B. Wang, S. Hu, Y. Teng, J. Chen, H. Wang, Y. Xu, K. Wang, J. Xu, Y. Cheng, X. Gao, *Signal Transduct. Target Ther.* **2024**, *9*, 200; b) N. C. Seeman, H. F. Sleiman, *Nat. Rev. Mater.* **2017**, *3*, 17068; c) W. Fan, W. Tang, J. Lau, Z. Shen, J. Xie, J. Shi, X. Chen, *Adv. Mater.* **2019**, *31*, e1806381.
[3] a) J. A. Joyce, *Cancer Cell* **2005**, *7*, 513; b) O. Farc, V. Cristea, *Exp. Ther. Med.* **2021**, *21*, 96; c) V. Chew, H. C. Toh, J.-P. Abastado, *J. Oncol.* **2012**, *2012*, 608406.
[4] a) J. Dai, Y. Su, S. Zhong, L. Cong, B. Liu, J. Yang, Y. Tao, Z. He, C. Chen, Y. Jiang, *Signal Transduct. Target. Ther.* **2020**, *5*, 145; b) I. Vanmeerbeek, S. Naulaerts, J. Sprooten, R. S. Laureano, J. Govaerts, R. Trotta, S. Pretto, S. Zhao, S. T. Cafarello, J. Verelst, M. Jacquemyn, M. Pociupany, L. Boon, S. M. Schlenner, S. Tejpar, D. Daelemans, M. Mazzone, A. D. Garg, *Sci. Adv.* **2024**, *10*, eadm8660; c) S. M. Stanford, T. P. Nguyen, J. Chang, Z. Zhao, G. L. Hackman, E. Santelli, C. M. Sanders, M. Katiki, E. Dondossola, B. L. Brauer, M. A. Diaz, Y. Zhan, S. H. Ramsey, P. A. Watson, B. Sankaran, C. Paindelli, V. Parietti, A. G. Mikos, A. Lodi, A. Bagrodia, A. Elliott, R. R. McKay, R. Murali, S. Tiziani, A. N. Kettenbach, N. Bottini, *Sci. Adv.* **2024**, *10*, eadg7887.
[5] a) R. A. Cardone, V. Casavola, S. J. Reshkin, *Nat. Rev. Cancer* **2005**, *5*, 786; b) S. Paget, *Lancet* **1889**, *133*, 571.
[6] a) Y. Zhang, V. Pan, X. Li, X. Yang, H. Li, P. Wang, Y. Ke, *Small* **2019**, *15*, 1900228; b) M. DeLuca, Z. Shi, C. E. Castro, G. Arya, *Nanoscale Horiz.* **2020**, *5*, 182; c) M. Schäfer, S. Werner, *Nat. Rev. Mol. Cell Biol.* **2008**, *9*, 628.
[7] a) A. P. Lapteva, N. Sarraf, L. Qian, *J. Am. Chem. Soc.* **2022**, *144*, 12443; b) Y. Zhang, N. Hu, J. Xu, Z. Wang, *VIEW* **2024**, *5*, 20230062; c) C. Zhang, L. Ge, Y. Zhuang, Z. Shen, Z. Zhong, Z. Zhang, X. You, *Sci. China Inf. Sci.* **2018**, *62*, 61301.
[8] D. G. DeNardo, P. Andreu, L. M. Coussens, *Cancer Metastasis Rev.* **2010**, *29*, 309.
[9] a) L. Yang, Q. Tang, M. Zhang, Y. Tian, X. Chen, R. Xu, Q. Ma, P. Guo, C. Zhang, D. Han, *Nat. Commun.* **2024**, *15*, 4583; b) Y. Liu, Y. Zeng, L. Liu, C. Zhuang, X. Fu, W. Huang, Z. Cai, *Nat. Commun.* **2014**, *5*, 5393; c) Q. Chao, Y. Zhang, Q. Li, L. Jiao, X. Sun, X. Chen, L. Zhu, Q. Yang, C. Shang, R.-M. Kong, G.-C. Fan, Z.-L. Song, X. Luo, *Anal. Chem.* **2023**, *95*, 7723; d) K. Wei, M. He, J. Zhang, C. Zhao, C. Nie, T. Zhang, Y. Liu, T. Chen, J. Jiang, X. Chu, *Angew. Chem. Int. Ed.* **2023**, *62*, e202307025.
[10] F. C. Simmel, B. Yurke, H. R. Singh, *Chem. Rev.* **2019**, *119*, 6326.
[11] D. Y. Zhang, G. Seelig, *Nat. Chem.* **2011**, *3*, 103.
[12] J. Zhu, L. Zhang, S. Dong, E. Wang, *ACS Nano* **2013**, *7*, 10211.
[13] a) D. Y. Zhang, E. Winfree, *J. Am. Chem. Soc.* **2009**, *131*, 17303; b) P. Irmisch, T. E. Ouldridge, R. Seidel, *J. Am. Chem. Soc.* **2020**, *142*, 11451.
[14] a) X. Mao, M. Liu, Q. Li, C. Fan, X. Zuo, *JACS Au* **2022**, *2*, 2381; b) S. He, Z. Ge, X. Zuo, C. Fan, X. Mao, *NPG Asia Mater.* **2021**, *13*, 42.
[15] a) M. Peters, I. Rozas, I. Alkorta, J. Elguero, *J. Phys. Chem. B* **2003**, *107*, 323; b) M. D. Frank-Kamenetskii, S. M. Mirkin, *Annu. Rev. Biochem.* **1995**, *64*, 65.
[16] Y. Hu, A. Cecconello, A. Idili, F. Ricci, I. Willner, *Angew. Chem. Int. Ed.* **2017**, *56*, 15210.
[17] A. Idili, K. W. Plaxco, A. Vallée-Bélisle, F. Ricci, *ACS Nano* **2013**, *7*, 10863.
[18] J. Liu, Y. Lu, *J. Am. Chem. Soc.* **2007**, *129*, 9838.
[19] I. Ortiz de Luzuriaga, X. Lopez, A. Gil, *Annu. Rev. Biophys.* **2021**, *50*, 209.
[20] J.-L. Mergny, D. Sen, *Chem. Rev.* **2019**, *119*, 6290.
[21] A. Marchand, V. Gabelica, *Nucleic Acids Res.* **2016**, *44*, 10999.
[22] a) J. Dong, M. P. O'Hagan, I. Willner, *Chem. Soc. Rev.* **2022**, *51*, 7631; b) J. J. Li, W. Tan, *Nano Lett.* **2002**, *2*, 315.
[23] P. Alberti, J.-L. Mergny, *Proc. Natl. Acad. Sci. U. S. A.* **2003**, *100*, 1569.
[24] T. Li, S. Dong, E. Wang, *J. Am. Chem. Soc.* **2010**, *132*, 13156.
[25] Y. C. Huang, D. Sen, *Angew. Chem. Int. Ed.* **2014**, *53*, 14055.
[26] H. Shu, R. Zhang, K. Xiao, J. Yang, X. Sun, *Biomolecules* **2022**, *12*, 648.
[27] P. Zhang, A. Fischer, Y. Ouyang, J. Wang, Y. S. Sohn, R. Nechushtai, E. Pikarsky, C. Fan, I. Willner, *Chem. Sci.* **2021**, *12*, 14473.
[28] H. A. Day, P. Pavlou, Z. A. E. Waller, *Bioorg. Med. Chem.* **2014**, *22*, 4407.
[29] A. L. Lieblein, J. Buck, K. Schlepckow, B. Furtig, H. Schwalbe, *Angew. Chem. Int. Ed.* **2012**, *51*, 250.
[30] a) M. Debnath, K. Fatma, J. Dash, *Angew. Chem. Int. Ed.* **2019**, *58*, 2942; b) H. Abou Assi, M. Garavís, C. González, M. J. Damha, *Nucleic Acids Res.* **2018**, *46*, 8038.
[31] a) E. Henke, R. Nandigama, S. Ergün, *Front. Mol. Biosci.* **2020**, *6*, 160; b) M. Wang, J. Zhao, L. Zhang, F. Wei, Y. Lian, Y. Wu, Z. Gong, S. Zhang, J. Zhou, K. Cao, X. Li, W. Xiong, G. Li, Z. Zeng, C. Guo, *J. Cancer* **2017**, *8*, 761.
[32] a) B. A. Webb, M. Chimenti, M. P. Jacobson, D. L. Barber, *Nat. Rev. Cancer* **2011**, *11*, 671; b) M. V. Liberti, J. W. Locasale, *Trends Biochem. Sci.* **2016**, *41*, 211; c) S. K. Vodnala, R. Eil, R. J. Kishton, M. Sukumar, T. N. Yamamoto, N.-H. Ha, P.-H. Lee, M. Shin, S. J. Patel, Z. Yu, D. C. Palmer, M. J. Kruhlak, X. Liu, J. W. Locasale, J. Huang, R. Roychoudhuri, T. Finkel, C. A. Klebanoff, N. P. Restifo, *Science* **2019**, *363*, eaau0135; d) G. K. Balendiran, R. Dabur, D. Fraser, *Cell Biochem. Funct.* **2004**, *22*, 343.
[33] H. Gong, Q. Dai, P. Peng, *ACS Appl. Mater. Interfaces* **2022**, *14*, 43026.
[34] P. Peng, Q. Wang, Y. Du, H. Wang, L. Shi, T. Li, *Anal. Chem.* **2020**, *92*, 9273.
[35] a) S. Das, M. Vera, V. Gandin, R. H. Singer, E. Tutucci, *Nat. Rev. Mol. Cell Biol.* **2021**, *22*, 483; b) G. J. Goodall, V. O. Wickramasinghe, *Nat. Rev. Cancer* **2021**, *21*, 22.
[36] a) D. Perrotti, P. Neviani, *Clin. Cancer Res.* **2007**, *13*, 1638; b) K. Ren, Y. Xu, Y. Liu, M. Yang, H. Ju, *ACS Nano* **2018**, *12*, 263.
[37] H. Wang, P. Peng, Q. Wang, Y. Du, Z. Tian, T. Li, *Angew. Chem. Int. Ed.* **2020**, *59*, 6099.
[38] L. Zhong, S. Cai, Y. Huang, L. Yin, Y. Yang, C. Lu, H. Yang, *Anal. Chem.* **2018**, *90*, 12059.
[39] Y. Zhao, Z. Li, B. Li, C. Wang, *Chem. Eur. J.* **2023**, *29*, e202301300.
[40] A. C. Mallory, H. Vaucheret, *Curr. Opin. Plant Biol.* **2004**, *7*, 120.
[41] B. DeVeale, J. Swindlehurst-Chan, R. Blelloch, *Nat. Rev. Genet.* **2021**, *22*, 307–323.
[42] L. Li, Y. Yu, C. Wang, Q. Han, X. Su, *Anal. Chem.* **2019**, *91*, 11122.
[43] J. Zhao, H. Chu, Y. Zhao, Y. Lu, L. Li, *J. Am. Chem. Soc.* **2019**, *141*, 7056.
[44] Q. Yang, F. Yang, W. Dai, X. Meng, W. Wei, Y. Cheng, J. Dong, H. Lu, H. Dong, *Adv. Healthc. Mater.* **2021**, *10*, 2101130.
[45] C. Zhang, Y. Zhao, X. Xu, R. Xu, H. Li, X. Teng, Y. Du, Y. Miao, H.-C. Lin, D. Han, *Nat. Nanotechnol.* **2020**, *15*, 709.
[46] a) C. X. Liu, X. Li, F. Nan, S. Jiang, X. Gao, S. K. Guo, W. Xue, Y. Cui, K. Dong, H. Ding, B. Qu, Z. Zhou, N. Shen, L. Yang, L.-L. Chen, *Cell* **2019**, *177*, 865; b) Q. Shang, Z. Yang, R. Jia, S. Ge, *Mol. Cancer* **2019**, *18*, 6.
[47] S. Bai, B. Xu, J. Wu, G. Xie, *Biosens. Bioelectron.* **2023**, *241*, 115677.
[48] a) S. Zalba, T. L. M. ten Hagen, *Cancer Treat. Rev.* **2017**, *52*, 48; b) R. H. Fang, A. V. Kroll, W. Gao, L. Zhang, *Adv. Mater.* **2018**, *30*, 1706759.
[49] R. Peng, X. Zheng, Y. Lyu, L. Xu, X. Zhang, G. Ke, Q. Liu, C. You, S. Huan, W. Tan, *J. Am. Chem. Soc.* **2018**, *140*, 9793.
[50] T. Song, S. Shah, H. Bui, S. Garg, A. Eshra, D. Fu, M. Yang, R. Mokhtar, J. Reif, *J. Am. Chem. Soc.* **2019**, *141*, 16539.
[51] X. Chang, C. Zhang, C. Lv, Y. Sun, M. Zhang, Y. Zhao, L. Yang, D. Han, W. Tan, *J. Am. Chem. Soc.* **2019**, *141*, 12738.
[52] a) J. Rak, A. Guha, *BioEssays* **2012**, *34*, 489; b) R. Xu, A. Rai, M. Chen, W. Suwakulsiri, D. W. Greening, R. J. Simpson, *Nat. Rev. Clin. Oncol.* **2018**, *15*, 617.
[53] Y. Li, J. Deng, Z. Han, C. Liu, F. Tian, R. Xu, D. Han, S. Zhang, J. Sun, *J. Am. Chem. Soc.* **2021**, *143*, 1290.
[54] a) R. Huang, P.-K. Zhou, *Signal Transduct. Target. Ther.* **2021**, *6*, 254; b) A. A. Kuznetsova, A. G. Matveeva, A. D. Milov, Y. N. Vorobjev, S. A. Dzuba, O. S. Fedorova, N. A. Kuznetsov, *Nucleic Acids Res.* **2018**, *46*, 11454; c) M. Afkhami, V. Sharma, M. Cuellar, M. D'Apuzzo, B. Badie, J. Portnow, R. K. Pillai, P. A. Aoun, M. Telatar, *J. Clin. Oncol.* **2016**, *34*, e23131.
[55] W. J. Zeng, X. R. Li, W. Liu, R. Yuan, W. B. Liang, Y. Zhuo, *Anal. Chem.* **2024**, *96*, 2117.
[56] a) J. W. Shay, W. E. Wright, *Nat. Rev. Genet.* **2019**, *20*, 299; b) S. B. Cohen, M. E. Graham, G. O. Lovrecz, N. Bache, P. J. Robinson, R. R. Reddel, *Science* **2007**, *315*, 1850.
[57] Z. Fan, J. Zhao, X. Chai, L. Li, *Angew. Chem. Int. Ed.* **2021**, *60*, 14887.
[58] J. Shi, M. Shen, W. Zhao, J. Liu, Z. Qu, M. Zhu, Z. Chen, P. Shi, Z. Zhang, S.-S. Zhang, *ACS Appl. Mater. Interfaces* **2021**, *13*, 51393.
[59] a) D. Yu, H. Pendergraff, J. Liu, H. B. Kordasiewicz, D. W. Cleveland, E. E. Swayze, W. F. Lima, S. T. Crooke, T. P. Prakash, D. R. Corey, *Cell* **2012**,

150, 895; b) W. F. Lima, T. P. Prakash, H. M. Murray, G. A. Kinberger, W. Li, A. E. Chappell, C. S. Li, S. F. Murray, H. Gaus, P. P. Seth, E. E. Swayze, S. T. Crooke, *Cell* **2012**, *150*, 883.
[60] K. Ren, Y. Liu, J. Wu, Y. Zhang, J. Zhu, M. Yang, H. Ju, *Nat. Commun.* **2016**, *7*, 13580.
[61] Q. Jiang, S. Yue, K. Yu, T. Tian, J. Zhang, H. Chu, Z. Cui, S. Bi, *J. Nanobiotechnol.* **2021**, *19*, 288.
[62] S. Zhou, X. Du, F. Cui, X. Zhang, *Small* **2014**, *10*, 980.
[63] R. Yue, M. Chen, N. Ma, *ACS Appl. Mater. Interfaces* **2020**, *12*, 32493.
[64] a) X. Li, S. Lee, J. Yoon, *Chem. Soc. Rev.* **2018**, *47*, 1174; b) X. Li, S. Kolemen, J. Yoon, E. U. Akkaya, *Adv. Funct.* **2017**, *27*, 1604053.
[65] Y. Zhang, W. Chen, Y. Fang, X. Zhang, Y. Liu, H. Ju, *J. Am. Chem. Soc.* **2021**, *143*, 15233.
[66] a) P. Zhao, H. Li, W. Bu, *Angew. Chem. Int. Ed.* **2023**, *62*, e202210415; b) S. L. Li, P. Jiang, F. L. Jiang, Y. Liu, *Adv. Funct.* **2021**, *31*, 2100243.
[67] Z. Wang, J. Yang, G. Qin, C. Zhao, J. Ren, X. Qu, *Angew. Chem. Int. Ed.* **2022**, *61*, e202204291.
[68] a) E. O. Long, *Annu. Rev. Immunol.* **1999**, *17*, 875; b) S. Miyamoto, S. K. Akiyama, K. M. Yamada, *Science* **1995**, *267*, 883.
[69] a) M. Ramos-Casals, J. R. Brahmer, M. K. Callahan, A. Flores-Chávez, N. Keegan, M. A. Khamashta, O. Lambotte, X. Mariette, A. Prat, M. E. Suárez-Almazor, *Nat. Rev. Dis. Primers* **2020**, *6*, 38; b) S. Yan, Z. Luo, Z. Li, Y. Wang, J. Tao, C. Gong, X. Liu, *Angew. Chem. Int. Ed.* **2020**, *59*, 17332.
[70] S. Bi, W. Chen, Y. Fang, J. Shen, Q. Zhang, H. Guo, H. Ju, Y. Liu, *Angew. Chem. Int. Ed.* **2024**, *63*, e202402522.
[71] S. Bi, W. Chen, Y. Fang, Y. Wang, Q. Zhang, H. Guo, H. Ju, Y. Liu, *J. Am. Chem. Soc.* **2023**, *145*, 5041.
[72] a) P. Friedl, J. A. Zallen, *Curr. Opin.Cell Biol.* **2010**, *22*, 557; b) M. E. Birnbaum, J. L. Mendoza, D. K. Sethi, S. Dong, J. Glanville, J. Dobbins, E. Özkan, M. M. Davis, K. W. Wucherpfennig, K. C. Garcia, *Cell* **2014**, *157*, 1073; c) P. Skoglund, R. Keller, *Curr. Opin. Cell Biol.* **2010**, *22*, 589; d) M. Genander, J. Frisén, *Curr. Opin. Cell Biol.* **2010**, *22*, 611; e) H. Zhang, C. Gally, M. Labouesse, *Curr. Opin. Cell Biol.* **2010**, *22*, 575.
[73] a) R. Mayor, C. Carmona-Fontaine, *Trends Cell Biol.* **2010**, *20*, 319; b) S. Sakaguchi, T. Yamaguchi, T. Nomura, M. Ono, *Cell* **2008**, *133*, 775.
[74] R. Tang, Y. Fu, B. Gong, Y. Fan, H. H. Wang, Y. Huang, Z. Nie, P. Wei, *Angew. Chem. Int. Ed.* **2022**, *61*, e202205902.

Manuscript received: September 15, 2024
Revised manuscript received: October 17, 2024
Accepted manuscript online: October 21, 2024
Version of record online: ■■, ■■

REVIEW

This review introduces the basic components of dynamic DNA nanostructures and discusses the application of DNA logic circuits based on these structures in cancer diagnosis and treatment. These logic circuits use cancer markers or external stimuli as input signals and achieve accurate diagnosis and treatment of tumors through logical operations, showing their potential in the field of precision cancer medicine.

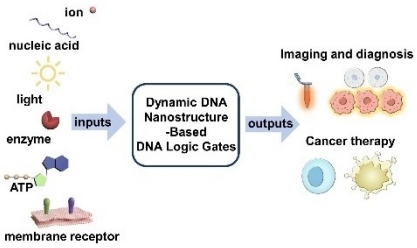

*S. Bi, R. Yang, H. Ju, Y. Liu**

1 – 15

Dynamic Nanostructure-Based DNA Logic Gates for Cancer Diagnosis and Therapy